Annals of Biomedical Engineering, Vol. 35, No. 6, June 2007 (© 2007) pp. 916–936
DOI: 10.1007/s10439-007-9266-1

Multi-cell Agent-based Simulation of the Microvasculature to Study the Dynamics of Circulating Inflammatory Cell Trafficking

ALEXANDER M. BAILEY, BRYAN C. THORNE, and SHAYN M. PEIRCE

Department of Biomedical Engineering, University of Virginia, PO Box 800759 Charlottesville, VA 22908, USA

(Received 22 September 2006; accepted 23 January 2007; published online 10 April 2007)

Abstract—Leukocyte trafficking through the microcirculation and into tissues is central in angiogenesis, inflammation, and the immune response. Although the literature is rich with mechanistic detail describing molecular mediators of these processes, integration of signaling events and cell behaviors within a unified spatial and temporal framework at the multi-cell tissue-level is needed to achieve a fuller understanding. We have developed a novel computational framework that combines agent-based modeling (ABM) with a network flow analysis to study monocyte homing. A microvascular network architecture derived from mouse muscle was incorporated into the ABM. Each individual cell was represented by an individual agent in the simulation. The network flow model calculates hemodynamic parameters (blood flow rates, fluid shear stress, and hydrostatic pressures) throughout the simulated microvascular network. These are incorporated into the ABM to affect monocyte transit through the network and chemokine/cytokine concentrations. In turn, simulated monocytes respond to their local mechanical and biochemical environments and make behavioral decisions based on a rule set derived from independent literature. Simulated cell behaviors give rise to emergent leukocyte rolling, adhesion, and extravasation. Molecular knockout simulations were performed to validate the model, and predictions of monocyte adhesion, rolling, and extravasation show good agreement with the independently published corresponding mouse studies.

Keywords—Microcirculation, Agent-based model, Network flow model, Monocyte, Inflammation, Leukocyte adhesion.

ABBREVIATIONS

EC	Endothelial cell
SMC	Smooth muscle cell
WSS	Wall shear stress
NO	Nitric oxide
IL-1β	Interleukin-1β
IL-4	Interleukin-4
IL-8	Interleukin-8
TNF-α	Tumor necrosis factor-α
VCAM-1	Vascular cell adhesion molecule-1
ICAM-1	Intercellular adhesion molecule-1
PSGL-1	P-selectin glycoprotein-1
LFA-1	Leukocyte functional antigen-1
VLA-4	Very late antigen-4

INTRODUCTION

Many vascular-associated pathologies and injury states are associated with inflammation, including atherosclerosis, stroke, chronic wounds, and peripheral vascular disease. Monocytes and other leukocytes are critical players in these diseases, where they have been shown to contribute to angiogenesis and microvascular remodeling,[8,21,64] atherosclerotic lesion progression and propensity to rupture,[6,7,58] as well as capillary plugging and tissue edema.[32,43,99] In cases of rampant inflammation, the participation of inflammatory cells can have an overall deleterious impact on the tissue. Therefore, limiting leukocyte participation may have desired therapeutic effects.[61] On the other hand, inflammatory cells also perform beneficial roles in mediating tissue recovery and regeneration,[25,64] and efforts to harness their therapeutic potential have garnered considerable attention, as in the case of ischemic pre-conditioning.[46,47] All of these effects are predicated on the ability of inflammatory cells to navigate through the microvasculature and preferentially home to sites of injury via interactions with the endothelium. Thus, understanding the role of inflammatory cells in vascular-associated pathologies necessitates a close study of leukocyte adhesion and the dynamics of this phenomenon as they manifest at the multi-cell tissue-level. To this end, we have developed an *agent-based computational model* that is underpinned by a *network blood flow simulation* to enable dynamic tracking of simulated inflammatory cells as they traffic through a microvascular network

Address correspondence to Shayn M. Peirce, Department of Biomedical Engineering, University of Virginia, PO Box 800759 Charlottesville, VA 22908, USA. Electronic mail: speirce@virginia.edu

Alexander M. Bailey and Bryan C. Thorne contributed equally to this work.

and home to a simulated muscle tissue bed. We then used our model to systematically interrogate the complex array of molecular signals that mediate this process with the goal of establishing a useful framework for further study of inflammatory cell participation in different disease settings.

Leukocyte–endothelial interactions are complex and dynamic—involving a cascade of molecular, mechanical, and biochemical signaling events, as well as spatially and temporally coordinated cell behaviors.[105] This complexity, along with limitations in *in vivo* cell tracking through the circulation and interstitial tissue space, as well as an inability to dynamically visualize *in vivo* tissues with sub-cellular resolution, has hampered progress towards a complete understanding of this process. We submit that available experimental techniques alone do not allow for thorough study of leukocyte trafficking in its entirety, and a computational systems biology approach capable of integrating multiple factors in space and time to produce tissue-level predictions is merited.

Leukocyte adhesion under flow conditions has been studied experimentally using intravital microscopy of animal cremaster muscles[19,63,112] and mesenteric tissue,[13] as well as in *in vitro* flow chamber assays that allow precise manipulation of soluble chemokine levels and adhesion molecule presentation.[17,53,55] This research has yielded a tremendous amount of detailed mechanistic data, and it has been demonstrated that for a generalized leukocyte population, adhesion tends to occur in sequential steps: (1) the capture of a flowing leukocyte out of the free-stream and onto the endothelium; (2) the subsequent formation and breaking of selectin bonds leading to rolling along the endothelium; (3) activation of leukocyte integrins by soluble and endothelial surface-bound chemokines; (4) firm adhesion of the leukocyte to the endothelium via activated integrins; and (5) trans-endothelial migration (for review see Ref.[59]). Inhibiting any one of these steps can lead to a failure of the entire process and greatly reduced trans-endothelial migration. For example, neutrophils will fail to progress through the adhesion cascade in the absence of selectins, whereas monocytes have been shown to be less dependent on selectin-mediated rolling and are able to transmigrate through integrin activation alone.[26,42] Traditionally however, it is believed that selectin-mediated rolling allows an inflammatory cell to 'survey' the endothelium for activating stimuli, which ultimately leads to integrin activation once a theoretical 'threshold activation level' is reached.[60] Thus, it is a unique pairing of molecular functionality that controls leukocyte adhesion: the selectins mediate the tethering and rolling of leukocytes, and the integrins utilize selectin-mediated rolling for more efficient activation and firm adhesion.

P- and E-selectins are found in endothelial cells (EC), although basal expression levels are very low. Within minutes of cell activation, both of these selectins are rapidly up-regulated and presented on the EC surface to their dominant ligand P-selectin glycoprotein-1 (PSGL-1) expressed on inflammatory cells (for a review of selectins see Ref.[62]). L-selectin is found only on inflammatory cells and also binds PSGL-1, although its main function is to allow circulating cells to survey and roll over each other.[104] The most well-studied integrins for leukocyte–endothelium firm adhesion are the $\beta 2$ integrins, MAC-1 and leukocyte functional antigen-1 (LFA1), and the $\alpha 4\beta 1$ integrin, very late antigen-4 (VLA-4) (for review see Refs.[66,94,113]). These integrins predominantly bind to vascular cell adhesion molecule-1 (VCAM-1) and intracellular adhesion molecule (ICAM-1), both of which are expressed on the surface of ECs.[85]

The progression through the adhesion cascade also depends on spatially and temporally regulated chemokine/cytokine behavior[59,105] and local hemodynamic forces (reviewed in Ref.[39]). The concentration of soluble and EC-surface-bound cytokines and chemokines has been shown to be critical in the activation of inflammatory cell integrins and modulation of adhesion molecule expression (reviewed in Refs.[48,51]). The mechanical influence of wall shear stress (WSS) has also been shown to modulate a rolling cell's velocity,[24] activate integrins,[75,116] and promote chemokine secretion from ECs.[65] Moreover, WSS values and flow velocities, if too large or small, may limit or prevent firm adhesion and/or rolling.[24,30,54] We have chosen to focus on these key inputs and signals as a first step towards developing a simulation of leukocyte trafficking at the multi-cell tissue-level scale.

Our multi-cell agent-based computational model (ABM) is coupled with a network blood flow analysis to allow the simulation of circulating inflammatory cell trafficking through the microvasculature while considering the effects of fluid flow and WSS. Combining these two computational approaches allowed for complex numerical analysis while preserving spatial and temporal tissue-level properties in order to predict degrees of leukocyte infiltration under varying conditions.

We applied our modeling framework to the process of monocyte trafficking through a skeletal muscle capillary bed. Blood flow exerts WSS at varying magnitudes and spatial distributions throughout the microvascular network, which influences adhesion molecule expression, chemokine/cytokine secretion, and the probability of wall interactions and bond formation. All of these properties interact to determine the dynamics of monocyte adhesion and transmigration. Our model is ideally suited for investigation of

this process. Consistent with literature, our simulations showed monocyte transmigration occurring primarily in the venules, even though no EC phenotypic differences in the vascular tree were explicitly programmed. Furthermore, simulated knockouts of L-selectin, both P- and E-selectins, and PSGL-1 preserved monocyte firm adhesion and transmigration levels, despite steep decreases in the instances of monocyte rolling. This is in agreement with *in vivo* experiments that indicate monocytes possess a decreased dependence on selectin-mediated rolling compared to neutrophils.[26] Simulated knockouts of individual integrins predicted varying degrees of dependence of firm adhesion on them, while knocking out both VCAM-1 and ICAM-1 resulted in no firm adhesion.

MATERIALS AND METHODS

Agent-based Modeling (ABM)

ABM is premised on the idea that local interactions between members of a population can lead to complex global outcomes. In ABM, a set of autonomous agents acting according to relatively simple rules give rise to, or predict, ''emergent'' phenomena that could not be discovered by probing the actions of one agent alone. Space and time are represented as discrete entities, and here simulations are conducted in a 2-dimensional space that is divided into a grid of stationary pixels in a Cartesian coordinate system. We use a ''cells-as-agents'' approach to ABM, wherein each individual agent represents one biological cell. Agents (cells) are motile within this coordinate grid and are able to survey and interact with their surrounding environment, including interactions with neighboring agents (cells) and the pixel space in which they move. Agents exhibit different behaviors (e.g., migration, division, death), and their attributes at any given time point can be described by an array of different state variables (e.g., expression levels of a particular protein, cell age).

As the simulation steps through time, individual agents make decisions about which behaviors to execute based on their states and those of their neighbors. Agents integrate these states using a literature-based rule set to determine what behaviors they should carry out. The state of each cell is followed over time, and cell actions, interactions, and cell fate/lineage are recorded for each agent. Interactions between agents and their environment give rise to altered tissue level properties over time, such as new structures and patterns that can be quantified using standard metrics (e.g., a newly remodeled microvascular network[84]). These properties of ABM make it ideally suited for investigation of biological systems where temporal and spatial outcomes at the tissue-level are important, as previously described in ABM models of inflammation,[3] microvascular network patterning,[84] and embryogenesis.[68]

Theoretical Modeling Framework

We approached the paradigm of leukocyte adhesion as being critically dependent on three general components: adhesion molecule expression, soluble and surface-bound chemokines/cytokines, and flow-mediated mechanical WSS forces. We believe the interactions between these components can accurately describe the spatial and temporal dynamics of leukocyte adhesion, from the initial capture and tethering to firm adhesion and transmigration. In order to model these processes computationally, so as to enable individual cell tracking and accurate hemodynamic profiles throughout a whole tissue bed, we developed a combined ABM and network flow model. The network flow model, implemented in MATLAB® (Version 7.0.4.352 (R14) Service Pack 2, MathWorks, Inc., Natick, MA), generated pressure changes, flow velocities, WSS, and varying viscosities within the simulated microvascular network. In turn, these parameters were loaded into the ABM and implemented in NetLogo,[110] versions 3.1 and 3.1.2, running on multiple workstations. They impact the flow path through the network of microvessels (driven by pressure differentials at bifurcations), and inform chemokine/cytokine secretion by individual cells, and individual monocyte interactions with the endothelium. All of the cellular responses to these inputs were programmed according to a literature-based rule-set (Tables 1–3), and this integrated approach is schematically represented in Fig. 1.

It is important to note that our framework allows for feedback between an individual cell's response to a changing mechanical force and the behaviors of neighboring cells, as depicted by the feedback loops between cell types and chemokine concentration levels in Fig. 1. Furthermore, the combination of adhesion molecule expression and chemokine/cytokine levels dynamically impact the probability of monocyte–EC interactions, integrin activation, and ligand–receptor binding—hence the grey arrow indicating communication between the two compartments of NetLogo in Fig. 1. Lastly, this theoretical modeling framework allows for firm adhesion to occur through different and not necessarily sequential pathways. For example, initiating firm adhesion without any selectin activity is possible, as is selectin-mediated rolling leading to integrin-mediated firm adhesion without any changes in adhesion molecule expression or circulating chemokine levels. Thus, we are able to investigate the cascade of leukocyte adhesion without prescribing the sequence of events leading to arrest.

TABLE 1. Adhesion molecule expression rules

Adhesion molecule	Surface expression levels	Literature-based rule	Citation
LFA-1 (CD11a)	Binding ligand	ICAM-1 (CD54)	72
	EC baseline (% pos. cells)	0%	22
	Monocyte baseline (% pos. cells)	100%	22
	Monocyte TNF-α-induced	No effect	115
MAC1 (CD11b, CD18)	Binding ligand	ICAM-1 (CD54)	15
	EC baseline (% pos. cells)	0%	22
	Monocyte baseline (% pos. cells)	100%	44
VLA-4 (CD49d, CD29)	Binding ligand	VCAM-1 (CD106)	23
	EC baseline (% pos. cells)	0%	34
	Monocyte (% pos. cells)	100%	35
ICAM-1 (CD54)	Binding ligand	LFA-1 (CD11a)	72,85,95
	EC baseline (% pos. cells)	66%	5,36,88,111
	EC WSS-induced	If WSS > 2 dynes/cm^2, 75%	4,75,78
	EC IL-1β-induced (+ exp. probability)	100%	31,78
	EC IL-4-induced (+ exp. probability)	25%	1,31
	EC TNF-α-induced (+ exp. probability)	90%	5,10,31,106
	Monocyte baseline (% pos. cells)	25%	20,95 (exact level assumed)
	Monocyte IL-1β induced (+ exp. probability)	75%	20
	Monocyte TNF-α induced (+ exp. probability)	50%	115
E-selectin (CD62e)	Binding ligand	PSGL-1 (CD162)	86
	EC baseline (% pos. cells)	3.25%	88
	EC WSS-induced (+ exp. probability)	No effect	75,78
	EC IL-1β-induced (+ exp. probability)	100%	12,78
	EC IL-4-induced (+ exp. probability)	4%	31,57
	EC TNF-α-induced (+ exp. probability)	50%	5,10,31
	Monocyte baseline (% pos. cells)	0%	22
L-selectin (CD62l)	Binding ligand	CD34, PSGL-1 (CD162)	104
	EC baseline (% pos. cells)	0%	22
	Monocyte baseline (% pos. cells)	90%	38,101
P-selectin (CD62p)	Binding ligand	PSGL-1 (CD162)	97
	EC baseline (% pos. cells)	5%	11,12,45,100,111
	EC IL-1β-induced (+ exp. probability)	30%	1,12
	EC IL-4-induced (+ exp. probability)	10%	1
	Monocyte baseline (% pos. cells)	0%	22
VCAM-1 (CD106)	Binding ligand	VLA-4 (CD29, CD49d)	23
	EC baseline (% pos. cells)	3.50%	111
	EC WSS-induced (+ exp. probability)	WSS < 1 dynes/cm^2, 30% 1 < WSS < 2 dynes/cm^2, 15% 2 < WSS < 4 dynes/cm^2, –20% WSS > 4 dynes/cm^2, –50%	4,28,78,80
	EC IL-1β-induced (+ exp. probability)	10%	73,78
	EC IL-4-induced (+ exp. probability)	40%	1,28,57,106
	EC TNF-α-induced (+ exp. probability)	60%	1,28
	EC NO induced (+ exp. probability)	5% if also IL-1β stimulated	14
	EC NO DF induced (+ exp. probability)	30% if also TNF-α stimulated	14
	Monocyte baseline (% pos. cells)	0%	22
PSGL-1 (CD162l)	Binding ligand	P-sel, E-sel, L-sel (CD62e,p,l)	97,104
	EC baseline (% pos. cells)	0%	104
	Monocyte baseline (% pos. cells)	100%	74

An expanded version of this table can be found at http://www.bme.virginia.edu/peirce.

Microvascular Network Acquisition

The following animal procedures were approved by the Animal Care and Use Committee of the University of Virginia. Confocal microscopy images of immunostained thin whole-mounted skeletal muscle tissues (from three spinotrapezius muscles of C57/BL6 male mice) were obtained, according to previously published methods[81]. These methods uniquely allow *en face* visualization of entire skeletal muscle microvascular beds with single cell resolution. Briefly, following anesthetization and euthanasia, spinotrapezius muscles were exteriorized, harvested, and fixed on gelatin-coated slides in methanol at 4 °C for 20 min. The tissues were then washed in a mixture of PBS + 0.1%

TABLE 2. Chemokine/cytokine activation rules

Chemokine/Cytokine	Activation	Literature-based rule	Citation
Interleukin-1β	Baseline blood level	0 units/plasma agent	[16,52]
	WSS-induced EC secretion	WSS < 2 dynes/cm^2, 0 units 2 < WSS < 4 dynes/cm^2, 300 units WSS > 4 dynes/cm^2, 850 units	[40]
	TNF-α-induced EC secretion	150 units	[67]
	IL-4-induced EC secretion	None	[85]
Interleukin-4	Baseline blood level	0 units/plasma agent	Arbitrary
	Inflammatory insult	0 units	Arbitrary
Interleukin-8	Baseline blood level	0 units/plasma agent	[109]
	WSS-induced EC secretion	WSS > 4 dynes/cm^2, 500 units	[65] (exact level assumed)
	IL-1β-induced EC secretion	700 units	[37]
	NO-induced EC secretion	None	[14]
	NO + IL-1β-induced-EC secretion	350 units	[14]
TNF-α	Baseline blood level	0 units/plasma agent	[87,96], Set to 0 arbitrarily
NO	Baseline blood level	0 units/plasma agent	[52,80]
	WSS-induced EC secretion	WSS < 1 dyne/cm^2, then 100 units 1 < WSS < 2 dynes/cm^2, 400 units 2 < WSS > 4 dynes/cm^2, 800 units WSS > 4 dynes/cm^2, 1200 units	[80]
All	Each time-step	[Chemokine] half-life = 1 program step	Estimated

An expanded version of this table can be found at http://www.bme.virginia.edu/peirce.

TABLE 3. Integrin activation and bond formation rules

Adhesion molecule	Activator	Literature-based rule	Citation
LFA-1 (CD11a)	WSS > 2 dynes/cm^2	3% integrins activated	[79]
	WSS > 2 dynes/cm^2 and MAC1 present	8% integrins activated	[79]
	IL-8	40% integrins activated	[29,69]
	Ligated L-selectin and MAC1 present	50% integrins activated	[29]
	Ligated E-selectin	No direct effect	[29]
VLA-4 (CD49d, CD29)	WSS < 2 dynes/cm^2	30% integrins activated	[116]
	2 dynes/cm^2 < WSS < 4 dynes/cm^2	22% integrins activated	[116]
	WSS > 4 dynes/cm^2	10% integrins activated	[116]
MAC1 (CD11b, CD18)	WSS > 2 dynes/cm^2	5% integrins activated	[79]
	WSS > 2 dynes/cm^2 and LFA-1 present	8% integrins activated	[79]
	Ligated L-selectin and LFA-1 present	50% integrins activated	[102]
	Ligated E-selectin	No direct effect	[29]
	IL-8	20% integrins activated	[29,69]
Selectins (CD62e,p,l)	WSS < 1 dynes/cm^2	50% endothelium interaction	[2,9,14,28,45,56,98,114]
	1 < WSS < 2.5 dynes/cm^2	100% endothelium interaction	[2,9,14,28,45,56,98,114]
	2.5 < WSS < 4 dynes/cm^2	25% endothelium interaction	[2,9,14,28,45,56,98,114]
	WSS > 4 dynes/cm^2	0% endothelium interaction	[2,9,14,28,45,56,98,114]
Integrins	Critical WSS > 7 dynes/cm^2	0% bond formation	[103] parameterized

An expanded version of this table can be found at http://www.bme.virginia.edu/peirce.

Saponin (4×20 min) before incubation with antibodies at room temperature for 18 h. Additional washes (4×20 min) were conducted in between primary and secondary antibody incubations, as well as after all staining was completed. ECs were identified using isolectin GS-IB$_4$ conjugated to Alexa-568 (Molecular Probes; 1:200) antibodies. Perivascular cells were identified with rabbit anti-NG2 chondroitin sulfate proteoglycan polyclonal antibody (Chemicon International; 1:100) with Cy2-conjugated goat (anti-rabbit) IgG secondary antibody (Jackson ImmunoResearch; 1:200). Inflammatory cells occupying the tissue space were identified using CD11b rat monoclonal (Serotec; 1:200) with Streptavidin-conjugated Alexa488 secondary antibodies (Molecular Probes; 1:200). Prior to staining, circulating cells were removed from the vasculature by perfusing vessels with heparanized 0.9% saline. CD11b is a surface antigen expressed on

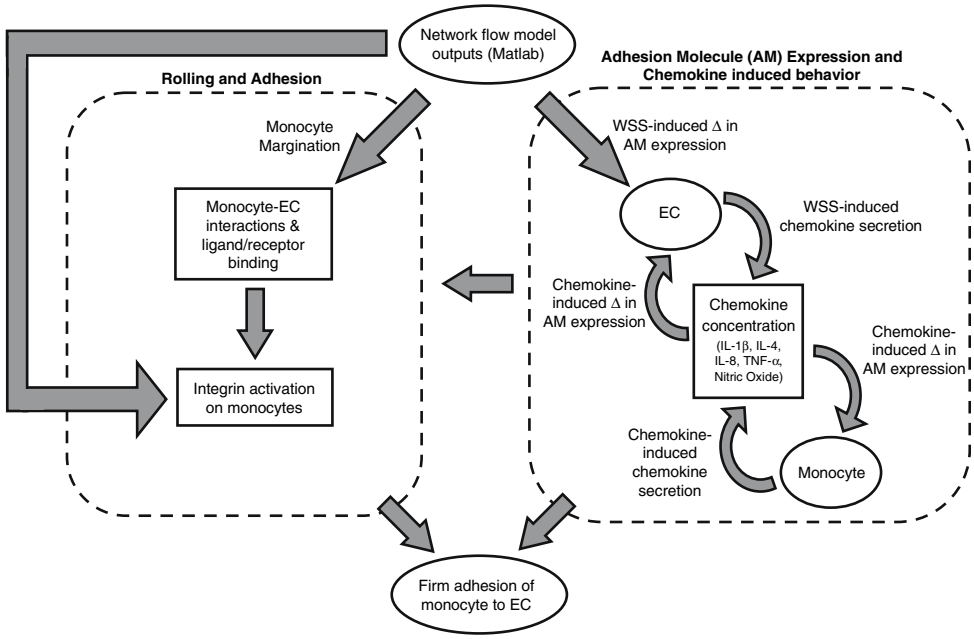

FIGURE 1. Schematic depicting theoretical modeling framework. The ABM component of the model (bounded by dashed lines) receives input from the network flow model component. Feedback loops between rule-sets allow complex behavior and determine a cell's ability to firmly adhere to the endothelium under a variety of conditions.

monocytes, tissue macrophages, and granulocytes and tissue macrophages. Digital images of immuno-labeled whole mount spinotrapezius tissue were acquired using confocal microscopy (Nikon, Model TE200-E2 with 20× objective).

ABM Initialization

From the confocal immunohistochemistry images, we selected a characteristic microvascular network. This network was discretized into nodes (branch-points) and elements (vessels) and manually drawn into the model window in NetLogo. Vessel characteristics were noted on the micrograph and inputted into NetLogo as individual features of each simulated vessel in the network. Specifically, vessel types (arteriole, venule, or capillary) were determined according to vessel diameter and wrapping morphology of the perivascular cells. Vessels with outer diameters less than or equal to 10 μm were classified as capillaries; vessels greater than 10 μm in diameter containing tightly wrapped perivascular cells (immunolabeled with NG2) were classified as arterioles; and vessels greater than 10 μm in diameter with loosely enwrapped perivascular cells were classified as venules.[77] Vessel lengths were calculated based on the number of EC (agents), which were assumed to be 25 μm in average length. Internal (luminal) vessel diameters were estimated from microvascular network confocal images. Pressures at the inlet and two outlets of the network were prescribed based on a range of physiological values.[108] Diameters, vessel lengths, capillary bed size (~1 mm distance from main feeding arteriole to draining venule), and pressures were consistent with *in vivo* observations and those found in literature[89,108] (Table 4).

Network Blood Flow Analysis

Blood flow through the microvasculature was simulated by implementing a model of network blood flow.[91,92] This model consists of two parts: solving for pressure and flows in a network (termed linear analysis by Pries and Secomb[91]) and applying empirically derived relationships to the solution to recalculate boundary conditions (termed "rheological analysis"[91]). This process is then iterated until a suitably small change in viscosity occurs. By discretizing a vascular network into nodes and elements and assuming low Reynolds number flow through a rigid and cylindrical tube, we computed the flow (Q) and pressures (P) throughout the theoretical vascular network. These assumptions allowed us to apply the finite element method to the network using Poiseuille's law (Eq. 1), a simplification of the Navier–Stokes equations. The rheological analysis takes into account microvascular phase separation effects,[92] and so viscosity was not assumed to be constant. Boundary conditions for Poiseuille's law included inlet and outlet pressures (Table 4), along with an initial estimate of viscosity.

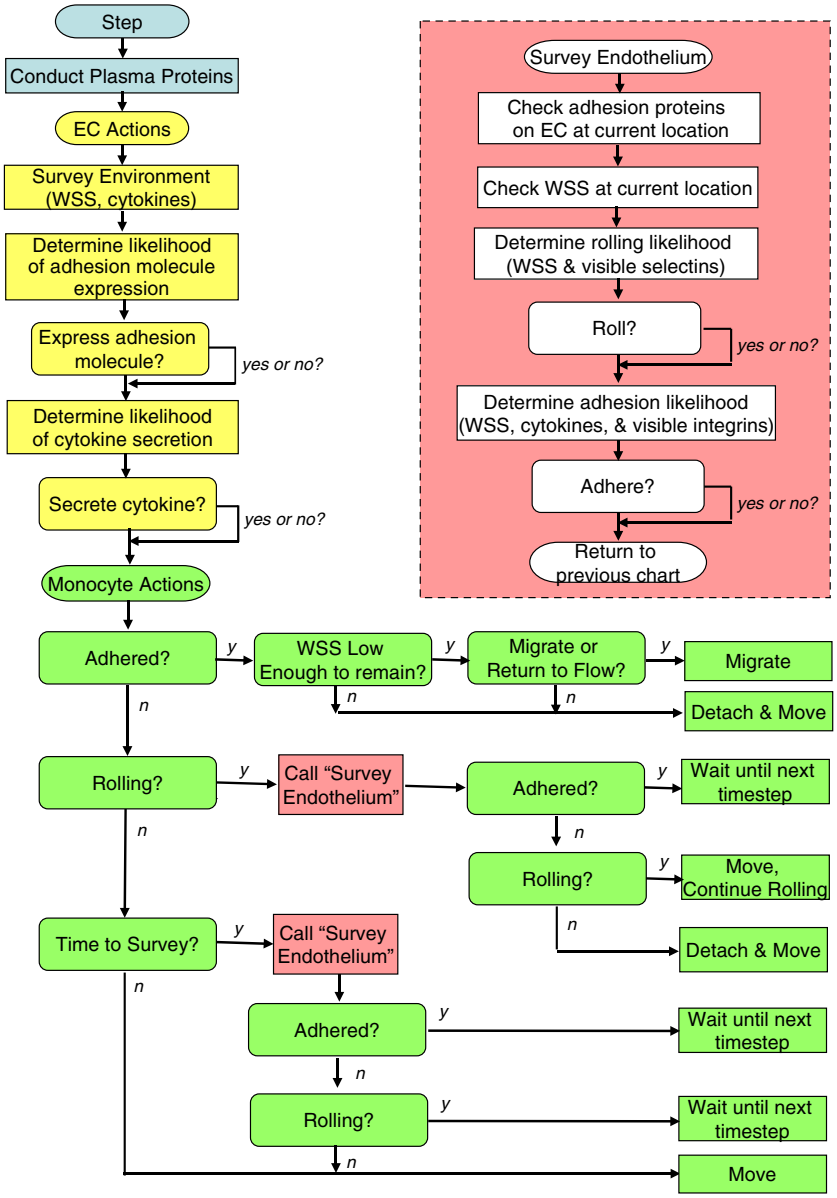

FIGURE 2. Flowchart of logic flow, cell actions, and decision points in the model. At each timestep, the model proceeds by conducting plasma proteins one step through the network. Each EC then performs the "EC Actions" portion of the flowchart (yellow), with decisions on expression of adhesion molecules and secretion of plasma proteins repeated without interruption for each protein. Next, each monocyte performs all of its actions (green). At key points, the monocyte surveys the endothelium (pink inset) and makes decisions about whether to roll or firm adhere. Processes are shown as rectangles, while decision points have rounded corners and y/n to indicate possible outcomes of the decision.

Our analysis required that the flows present at any node in the network must sum to zero, as dictated by the law of conservation of mass.

$$Q = \frac{\pi R^4 \Delta P}{8 \mu_{\text{app}} L} \tag{1}$$

and

$$\sum Q_{(i,j)} = 0 \tag{2}$$

where μ_{app} is the apparent viscosity.

Erythrocyte (assumed to be identical to monocyte distributions in our model) distributions at divergent bifurcations are not linearly proportional to plasma blood flow, so our simulation used Eqs. (3)–(7)[91] to relate the fraction of total red blood cells flowing in a feeding vessel (FQ_E) to the fractional blood flow entering a downstream vessel (FQ_B) at a bifurcation. These equations enabled the calculation of FQ_E with a known feed vessel hematocrit (H_F) and diameter (D_F), known fractional blood flow to the downstream vessel

TABLE 4. In silico microvascular network parameters.

	Avg. diameter (μm)	Avg. length (μm)	WSS (dynes/cm^2)	Fluid flow (mL/min)
Arteriole	11.36	454.55	4.82	0.016
Venule	14	604.17	1.37	0.028
Capillary	5.4	390	2.48	0.001
Capillary bed size	1 mm			
Average EC size	25 μm			
Pressures (mmHg)	20 at I-1 15 at O-1 16 at O-2			

(FQ_B), and known diameters of both downstream vessels (D_α and D_β).

$$\text{logit}(FQ_E) = A + B\text{logit}\left(\frac{FQ_B - X_0}{1 - 2X_0}\right) \tag{3}$$

$$\text{logit}(x) = \ln\left(\frac{x}{1-x}\right) \tag{4}$$

$$A = -6.96 \ln\left(\frac{D_\alpha}{D_\beta}\right)/D_F \tag{5}$$

$$B = 1 + 6.98\left(\frac{1 - H_F}{D_F}\right) \tag{6}$$

$$X_0 = \frac{0.4}{D_F} \tag{7}$$

$$H_{D1} = FQ_{ED1}\frac{(H_F Q_F)}{Q_{D1}} \tag{8}$$

Fractional red blood cell flow (FQ_E) into each downstream vessel at a bifurcation was used to calculate hematocrit in that segment using Eq. (8) where H_{D1} is the hematocrit in the downstream vessel. At convergent bifurcations, downstream vessel hematocrit (H_D) was calculated when downstream vessel flow rate (Q) as well as the hematocrit and flow rates in the two parent vessels were known (H_{D1}, H_{D1} and Q_1, Q_2), using conservation of mass (Eq. 9).

$$H_D = \frac{H_{D1}Q_1 + H_{D2}Q_2}{Q} \tag{9}$$

Vessel hematocrit was then used together with Pries and Secomb's[92] "*in vivo* viscosity law" to calculate apparent vessel viscosity as a function of the diameter of the vessel (D) and the discharge hematocrit (H_D: Eqs. 10–12).

$$\eta_{vivo} = \left[1 + (\eta^*_{0.45} - 1)\cdot\frac{(1-H_D)^C - 1}{(1-0.45)^C - 1}\cdot\left(\frac{D}{D-1.1}\right)^2\right]\cdot\left(\frac{D}{D-1.1}\right)^2 \tag{10}$$

$$C = (0.08 + e^{-0.075D})\cdot\left(-1 + \frac{1}{1 + 10^{-11}\cdot D^{12}}\right) + \frac{1}{1 + 10^{-11}\cdot D^{12}} \tag{11}$$

$$\eta^*_{0.45} = 6\cdot e^{-0.085D} + 3.2 - 2.44\cdot e^{-0.06D^{0.065}} \tag{12}$$

WSS between nodes i and j, τ_{ij} was calculated according to Eq. (13).[89]

$$\tau_{ij} = (P_i - P_j)\frac{d_{ij}}{4L_{ij}} \tag{13}$$

Integration of ABM and Network Flow Models

To integrate the ABM and network flow models, we developed an extension to NetLogo that calls the network flow analysis, implemented in MATLAB®, pauses NetLogo execution, and resumes execution in NetLogo upon receipt of the results. The NetLogo model writes relevant information about each element (length, diameter, node connectivity), known nodal pressures, and estimated blood viscosity to a file. The NetLogo model then calls MATLAB® to execute a script that reads in the file, performs flow analysis at that time-point, and writes nodal pressures, elemental flows, and WSS to a second file. Execution returns to NetLogo, which reads the output from MATLAB®, assigns fluid flows and WSS to branches of the vascular network, and pressures at each bifurcation. The model assumes that WSS at the bifurcations of the vessels is the average of WSS in neighboring vessels. It further assumes the pressure drop along each segment is linear and assigns a point pressure to each endothelial cell agent. It is this pressure differential between neighboring ECs that is used to drive leukocyte movement through blood vessels. It is important to note that the flow of plasma and circulating cells was based entirely on the inputs of experienced mechanical forces derived from the network flow model and that circulating cells are not explicitly programmed to flow through the vascular tree from arteriole to venule. The capability exists to recalculate pressure, flow, and WSS from within a running model if a change in network connectivity is detected. This feature would be important for future models that incorporate angiogenesis and

result in the generation of new vessels within the microvascular network.

Cell Types, Adhesion Molecules, and Cytokines

Within the ABM we allowed for complex interactions between ECs and monocytes. Smooth muscle cells (SMCs) are also present, although as yet they have no behavioral rules. Each cell (agent) carries binary information regarding its instantaneous adhesion molecule expression (P-, E-, L-selectins, VCAM-1, ICAM-1, PSGL-1, VLA-4, LFA-1, MAC-1), as well as scaled chemokine and cytokine exposure (TNF-α, IL-1β, IL-4, IL-8, NO). To accommodate circulating soluble chemokine/cytokine levels we created a separate plasma agent, which carries soluble molecule concentrations through the microvascular network.

Description of Model Execution

The flowchart in Fig. 2 visually represents the logic flow through the model and the decisions made by each cell type for a given step in the simulation. At each time step, ECs survey their environment and express adhesion molecules or secrete chemokines/cytokines according to a rule set (Tables 1–3). Monocytes enter the microvascular network at an inlet node and survey their local environment. Like the EC, the monocyte then determines its expression profile and surveys the endothelium for the ligands of its adhesion molecules. If WSS is within a specified range (Table 3) and the proper selectins are present (Table 1), the monocyte begins rolling. Rolling serves to decrease monocyte travel speed through the vessel and increase the rate at which it surveys the vessel wall for adhesion molecules. Monocytes also check for integrin expression and activation to determine whether or not to arrest (Table 3).

Adhesion Molecule Expression

Expression of adhesion molecules is determined by the rules shown in Table 1. Expression is calculated at each time step and is assumed to be instantaneous. When a cell detects a cytokine or WSS level that would change adhesion molecule expression levels, it changes the expression level at that time step, with no delay for internal signaling or protein synthesis. If more than one influence on the expression of a certain molecule is present, expression is determined in a non-additive manner: the value for the cytokine with the largest influence on expression is used. A WSS modifier is applied to this value, followed by the application of a nitric oxide (NO) modifier if any NO is present. Cell surface expression is handled in a binary manner; either a cell expresses a molecule or it does not. See Table 1 for the full list of rules and citations.

Within our rule-set (Table 1), E-selectin is expressed by 3.25% of ECs and is not expressed by monocytes. Contact with Il-1β induces E-selectin expression by ECs with a probability of 100%, Il-4 induces E-selectin expression with a probability of 4%, and TNF-α induces E-selectin expression with a probability of 50%. IL-8 and varying WSS have no effect on expression levels (Table 2).

VCAM-1 is also expressed on ECs at a baseline of 3.5% of cells, although it is not expressed on monocytes. Chemokine/cytokine influences on expression are similar to those for E-selectin (Table 1), and increasing WSS values decrease expression of VCAM-1. NO also decreases the expression of VCAM-1. If NO is encountered, the likelihood of positive VCAM-1 expression is reduced by 50%, even after chemokine/cytokine and WSS influences. Expression for other adhesion molecules is carried out in a similar manner (Tables 1 and 2).

As with any computer simulation based on rules obtained from independent experimental literature, careful attention must be paid to the consistency and correctness of reported parameter values that will be incorporated into the simulation. For this reason, when possible, multiple publications were referenced for each individual rule. We then evaluated important aspects of the reported data and experimental design from each publication in order to arrive at a rule or value that accurately reflects the field's understanding as a whole, to the best of our knowledge. For example, when determining the percent of ECs in our simulation that should express a certain adhesion molecule at baseline levels, there were often discrepancies present in the literature. If *in vivo* immunofluorescence data of mouse microvascular ECs showing quantifiable expression of an adhesion molecule was unavailable, we would next consider microvascular ECs from a similar species, such as rat or human. In the cases where this type of data was unavailable, we would look at *in vitro* data in another experimental system such as flow cytometry. Similarly, we would consider the expression data on ECs isolated from large vessels or lung microvessels only when data from microvascular skeletal muscle ECs was unavailable. Values were often averaged, and a similar approach was applied to determine all the rules incorporated into this simulation.

Secretion of Soluble Factors

Simulated soluble molecules include IL-1β, Il-8, IL-4, TNF-α, and NO. We selected these key molecules from among the many cytokines that are known to play important roles in regulation of adhesion

molecules. Factors affecting secretion of these molecules and their relative values are shown in Table 2. Values were taken from the literature and adjusted to an arbitrary 1000-point scale as a percent chance for a cell at that time point to sense a cytokine, based on relative potency and amounts secreted. For example, if a survey of the literature indicated that IL-4-induced secretion of IL-1β by EC was 3–5 times less effective than IL-1β-induced secretion of IL-8 by EC, it would be given an appropriate relative number on the scale (see Table 2). When assigning an effectiveness to a chemokine, the potency, time to onset, acting time, and experimental conditions were factored into the judgment to resolve any discrepancies and determine relative behaviors. These rules in particular, therefore, need to be refined as additional experimental data becomes available and further parameterization is conducted. Note that while the capability for cells to respond to IL-4 and TNF-α exists in the model, these molecules are not included in the simulations described here. The effect of IL-4 and TNF-α could be turned on by setting a baseline plasma value in the model code, or by adding a cell type that would express them along with rules for their expression.

Secretion is programmed in the same general manner for each molecule. Briefly, ECs and monocytes survey their environment, checking WSS and plasma levels of cytokines. They then calculate secretion levels in a non-additive manner, taking the maximum secretion amount from all the currently active factors influencing production (Table 2, Fig. 2). Cells secrete soluble molecules by transferring a fixed amount to the plasma agent adjacent to the cell. Plasma agents degrade all soluble factors by a fixed percentage at each time step. Rules shown in gray are less certain, and are potential targets for parameterization or further experimentation.

Secretion of NO by ECs in our model is based solely on WSS (Table 2). As WSS increases, more NO is secreted. The numeric values of WSS are divided up into four levels, and rules for each level are shown in Table 3. IL-8 secretion is induced by both high WSS and IL-1β levels. After taking the maximum of these stimuli, if the EC has encountered NO at the current time step, it reduces its secretion of IL-8 by 50%. Secretion of other soluble factors is handled in a similar manner (Table 2).

Leukocyte Rolling

The likelihood of a cell rolling on the endothelium is determined by a combination of WSS and selectin expression at discrete locations within the network. A circulating cell first checks the magnitude of WSS it is experiencing to determine how likely it is to roll if the proper adhesion molecules are in place (Table 3). It then checks to see whether it is expressing PSGL-1 and has been in the proximity of an endothelial cell expressing either E-selectin or P-selectin. It also checks to see whether it is expressing L-selectin and has been in contact with another rolling monocyte expressing PSGL-1. If any of these conditions are met, the probability rule described above is applied, and this determines whether or not the monocyte initiates rolling on the endothelium. Rolling cells survey the endothelium at every time-step, and move to the next EC at every other time-step. Non-rolling cells move at every time-step and survey the endothelium at a rate determined by the ratio between the calculated flow velocity at their location and the literature-defined velocity of a rolling cell.[41,54,93]

Cell Firm Adhesion

There are three possible ligand/receptor pairs that once bound can lead to cell arrest in this model: LFA-1/ICAM-1, MAC-1/ICAM-1, and VLA-4/VCAM-1. The affinity and binding rules for these integrins are shown in Table 3. Most of the published data reports the percentage of integrins on a single cell in a high affinity state in response to different treatments. We assume that percentage of high-affinity integrins on a single cell roughly translates to percent of total cells that will adhere given a certain treatment. The probability of a monocyte firm adhering is calculated separately for each integrin (LFA-1, MAC-1, VLA-4). In this model, VLA-4 binding probability depends mainly on WSS, while LFA-1 and MAC-1, having the same ligand, can cross-activate each other, and are activated by IL-8 and/or L-selectin ligation. The probabilities of integrin activation are compared, and the maximum value is used as the likelihood that a cell will firm adhere. At WSS greater than 7 dynes/cm^2, no arrest can occur in our model (Table 3). Because not all firmly adhered cells eventually complete extravasation, we assign firm adhered cells a 75% probability of re-entering the bloodstream.[33] This chance is applied during the cell's decision of whether to arrest.

Extravasation

Cells are assumed to extravasate from the microcirculation into the tissue after they have arrested for three time steps. This time was chosen because it has been shown[33] that arrested cells can extravasate on a timescale of seconds to minutes. It has also been shown that the majority of monocytes that migrate into the tissue (approximately 75%)[27,76] do not become tissue macrophages, but differentiate into another, more mobile cell type (possibly dendritic cells) and migrate

out of the tissue either via the lymphatic channels or the bloodstream. This is accommodated by removing these cells from the blood (they extravasate), but excluding them from the final analysis of total tissue macrophages. Cells that survive to become tissue macrophages migrate through the interstitial space in a random walk pattern at each timestep. In this version of the model, the number of tissue macrophages is used as an output metric only.

Time Steps

Time steps in the model are relative to one another, but arbitrary with respect to the actual amount of time required for cell transit through the circulation, ligand binding, etc. Because keeping track of prior activating influences on a cell and integrating them over time is computationally intensive, we have assumed instantaneous expression based on a cell's current environment and state. The output of the model can be viewed as a non-dimensionalized version of extravasation in which the behaviors of the individual cells represent a response to their time-averaged expression levels. Each model was run for 1500 time steps.

Simulations of Trafficking/Model Validation

We developed the rules for this model by considering data derived from *in vitro* and *in vivo* experiments. These data combine to constitute our rule-set, which governs individual cells' behavioral responses when confronted with environmental/neighbor–neighbor changes. For validation, we performed *in silico* knockout experiments and compared the tissue-level outcomes (specifically, the number of tissue macrophages) and degree of rolling predicted to those seen in *in vivo* knockout mice studies that are published in independent literature. In our model, we systematically and sequentially knocked out the following molecules and combinations of molecules: (1) E- and P-selectin, (2) L-selectin, (3) PSGL-1, (4) VCAM-1, and (5) ICAM-1. We also assessed the sensitivity of our model to changes in plasma protein degradation rates, frequency of surveying the endothelium when monocytes were located in the free stream and not rolling, and varying WSS levels. Each simulation was repeated five times.

Model Code

The NetLogo model file, the NetLogo extension, and the Matlab script have been placed online at http://www.bme.virginia.edu/peirce. Also at this location are expanded versions of Tables 1–3, including explanations for the derivation of rules, citation summaries, and justifications for the resolution of discrepancies between sources.

Statistics

All results are presented in the form of mean ± standard deviation. All comparisons were made using the statistical analysis tools provided by SigmaPlot 5.0 (Systat, Inc., Point Richmond, CA). Data were tested for normality and analyzed by one-way ANOVA followed by non-paired Tukey's *T*-test. Where unequal variances prevented analysis of a set of experiments as a whole, Student's *T*-test was used to compare individual experiments to control. Statistical significance was asserted at $p \leq 0.05$.

RESULTS

Communication between Network Flow and ABM Simulations

The network blood flow model calculated fluid flow velocities, pressure distributions, and WSS values in a simulated microvascular network (Table 4). Phase separation effects were not ignored as they play a critical role in determining blood viscosity throughout small diameter vessels. By accounting for changes in viscosity and assuming it to be variable with vessel length, diameter, and connectivity, the simulation was able to more accurately determine the mechanical parameters. The inputs for the network flow model were taken directly from the ABM drawing program in NetLogo, and the accurate segment length and nodal connectivity indicate successful communication between the two models.

Computational Model Allows Input of In Vivo Microvascular Architecture

Skeletal muscle capillary beds from the mouse spinotrapezius were obtained using confocal microscopy and inputted into the ABM drawing program while preserving network architecture, vessel lengths, vessel diameters, and connectivity (Figs. 3a and 3b). The simulation allows multiple blood flow outputs, as shown (two outputs), as well as multiple inputs (not shown). Arterioles and venules were simulated by ECs (yellow agents) bordered by SMCs (red agents). The capillaries possess no SMCs, either *in vivo* or within the simulation space and are simulated as single-file lines of ECs.

Monocytes Extravasate Predominantly at Venules

In silico experiments predict sites of monocyte transmigration in simulated microvascular beds, and

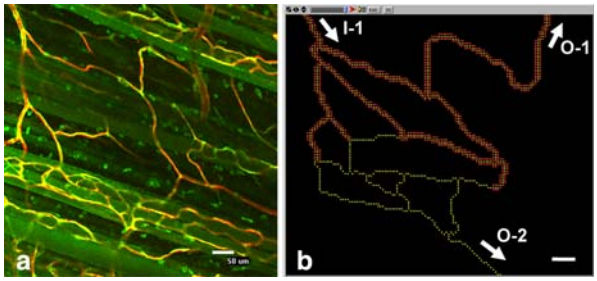

FIGURE 3. Method of obtaining a real microvascular network architecture for the agent-based simulation: (a) Confocal microscopy image of a whole-mounted mouse spinotrapezius muscle immunostained to visualize the microvascular network. ECs were identified with BSI-lectin antibody (red), and perivascular cells were identified with NG2 antibody (green). The micrograph was manually discretized into nodes, defined as bifurcation points in the microvascular network, and the nodes were connected to form elements. Nodes and elements were manually drawn into the NetLogo simulation space, as shown in the screen-shot (b), to represent the real microvascular network. Actual vessel lengths and diameters of each microvessel were measured on the micrograph and input into the NetLogo simulation. Arterioles and venules were characterized on the micrograph based on vessel diameter and the morphology of perivascular cell coverage (with tight perivascular cell wrapping indicating an arteriole). Simulated arterioles and venules contained ECs (yellow agents) bordered on both sides with SMCs (red agents), while capillaries (which lack mature SMC coverage) contained ECs (yellow agents) only. Arrows indicate inlet and two outlets and direction of flow in the *in silico* microvascualar network.

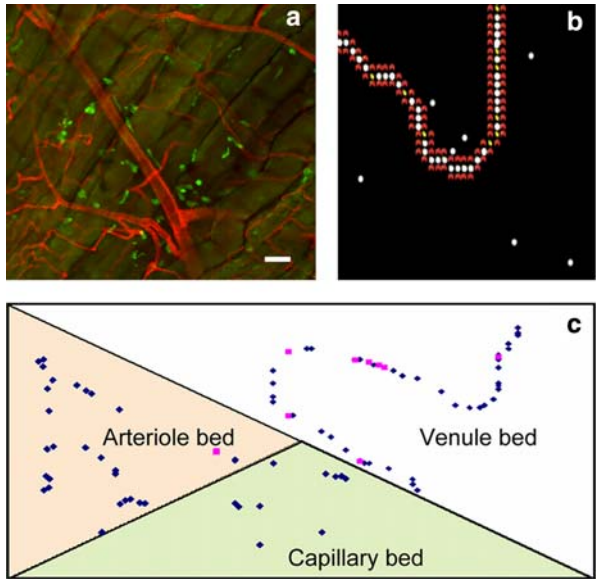

FIGURE 4. Comparison of spatial outcomes: (a) Confocal microscopy of ECs in a mouse spinotrapezius muscle immunolabeled with lectin (red) and leukocytes immunolabeled with CD11b (green) at 20× magnification. Vascular network properties including vessel order, location, and branching are evident as are the spatial positions of the leukocytes that have infiltrated the tissue. *In vivo* images like this can be used to validate spatial patterns predicted by the *in silico* experiments. Scale bar is 50 μm. (b) Sample screen shot from model simulation showing simulated venule and predictions for monocyte location (white-colored agents) following 1500 time-steps. Inherent in screen shots like this are data concerning spatial patterning which can be compared to *in vivo* findings. (c) X–Y plot showing the sites of firm adhesion and transmigration across a 1500-time-step simulation with the complete (control simulation) rule set. Monocytes that firm adhered independent of any rolling are depicted as blue diamonds. Monocytes that progressed from rolling to firm adhesion (and transmigration) are depicted as pink squares. Total monocyte extravasation occurred predominantly out of the venule bed relative to arteriole and capillary beds.

this can be compared directly to *in vivo* whole-mount confocal images of the mouse spinotrapezius stained for leukocytes and EC (Figs. 4a and 4b). In this way, it is possible to validate model predictions of the spatial patterns of monocyte extravasation with *in vivo* findings. This capitalizes on the strengths of ABM programs and will be instituted in future models for further validation.

Our simulations predicted leukocyte firm adhesion and transmigration occurring predominantly in the venule bed of the microvascular network, although these behaviors were also exhibited in both the capillary and arteriole beds (Fig. 4c). Figure 4c is a plot of the locations of monocyte extravasation divided into three areas: arteriole bed, capillary bed, and venule bed. Cells that firmly adhered without rolling are depicted as blue diamonds, while cells that progressed from rolling to firm adhesion are shown as pink squares. All simulations, including the selectin knockout trials, showed higher numbers of extravasated monocytes in the venule compartments, even after the elimination of selectin-mediated rolling (in the PSGL-1 and double E- and P-selectins knockouts). This is consistent with the current understanding that the majority of leukocyte adhesion occurs in activated venules where WSS values are lower and the proper adhesion molecules are presented to circulating cells. It is important to note that this prediction was not preprogrammed in the rule-set (e.g., a forgone conclusion), but emerged independently as a result of the actions and interactions of the agents responding to their dynamic simulated mechanical and biochemical environments.

Simulation Predicts Low Dependence of Monocytes on Selectins for Firm Adhesion

To validate our model, we simulated the effects of abolishing selectin activity by knocking out combinations of selectins and their ligand. All of these simulations predicted non-significant changes in the amount of extravasated monocytes (Fig. 5), despite graded reductions in the ability of a circulating cell to roll along the endothelium (Fig. 6). The L-selectin

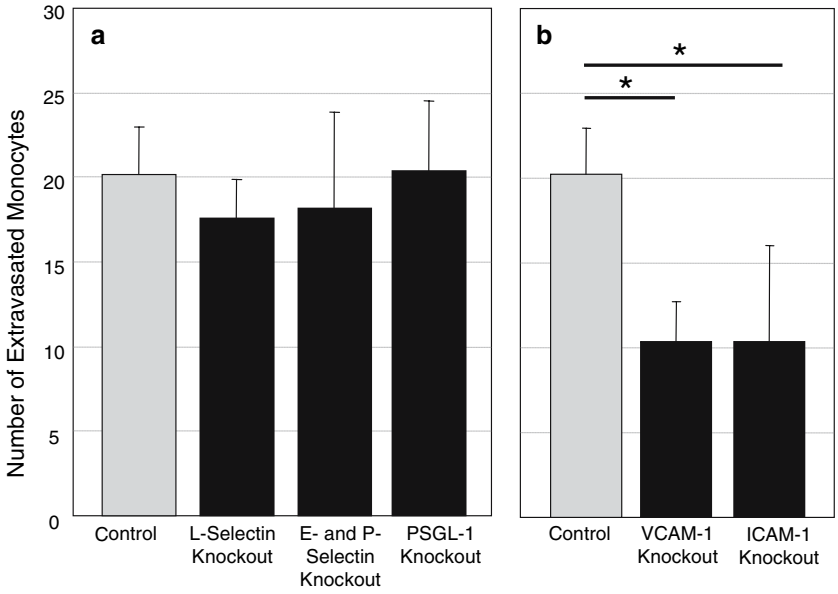

FIGURE 5. Number of extravasated monocytes in knockout simulations as compared to control simulation. *In silico* systematic knockout of selectins (a), and integrins (b). L-, E- and P-selectins, and PSGL-1 knockouts showed no significant differences from the control group. Knocking out either ICAM-1 or VCAM-1 caused a significant reduction in the number of extravasated monocytes compared to control (±SD; * = statistically significant relative to what the horizontal bars indicate with $p \leq 0.05$).

knockout showed approximately a 20% decrease in rolling, while the double (E- and P-selectins) and the PSGL-1 simulated knockouts showed a complete ablation of a cell's ability to roll along the endothelium (Fig. 6). The maintained extravasation levels are a non-intuitive result, which is consistent with the literature that indicates a decreased dependence of monocytes on selectin-mediated rolling for firm adhesion.[26,42] A critical next step is to match these *in silico* predictions with *in vivo* experimentation on selectin

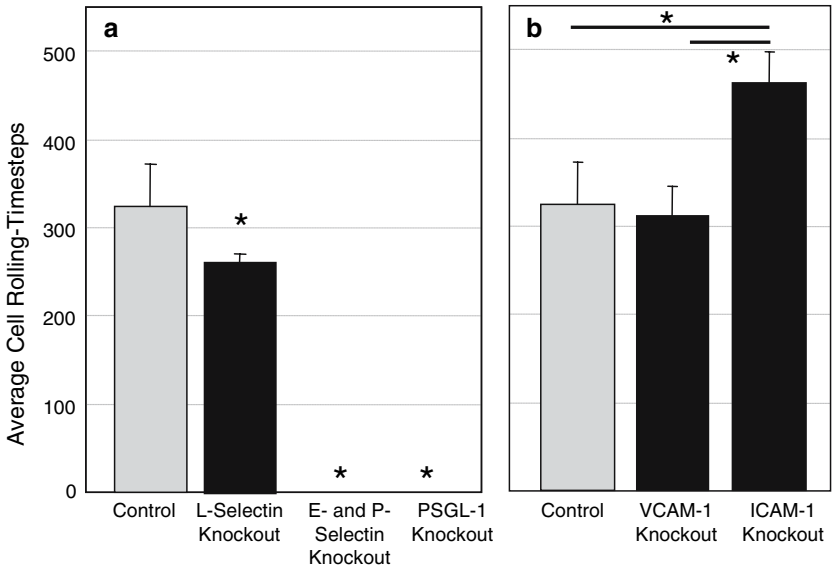

FIGURE 6. Rolling monocytes in different knockout simulations as compared to control simulation (reported as Cell Rolling-Timesteps; the number of cells that rolled in the simulation multiplied by the total timesteps each cell rolled). (a) *In silico* knockout of L-selectin showed approximately a 20% decrease in rolling from the control simulation, while knockouts of E- and P-selectins and PSGL-1 showed no rolling (or 100% decrease from control simulation), as expected (±SD; * = statistically significant compared to control using a Students *t*-test with $p \leq 0.05$). (b) VCAM-1 knockout showed no change in rolling, while ICAM-1 knockout showed a significant 42% increase in rolling, likely due to decreased cell adhesion (±SD; * = statistically significant relative to what the horizontal bars indicate with $p \leq 0.05$).

knockout animals using the spinotrapezius or cremaster muscle preparations where intravital microscopy paired with immunohistochemistry will permit such analysis. This will further validate our model and theoretical approach for capturing the progression of monocytes through the adhesion cascade.

The *in silico* knockouts of both ICAM-1 and VCAM-1 showed a significant reduction in the number of extravasated monocytes compared to control, (Fig. 5). Similarly, *in silico* ICAM-1 knockouts showed a 42% increase in rolling, while VCAM-1 knockouts showed no significant difference (Fig. 6). The *in silico* knockout of ICAM-1 *and* VCAM-1 showed no firm adhesion or transmigration, while selectin-mediated rolling was greatly increased (data not shown). This is likely due to the fact that because the integrins are required for firm adhesion, simulated cells are continuing to roll for longer time periods. These data suggest that integrins have a dominant role over selectins in the monocyte adhesion cascade.

Parameter Sensitivity Analysis

In order to examine the impact of different parameters on the model, we performed a detailed sensitivity analysis of the plasma protein degradation rate, the wall surveying rate for non-rolling cells, and the WSS. There was no significant impact of varying the protein degradation rate from 0 to 100% per timestep on total monocyte extravasation (Fig. 7a). However, there was a significant dose-dependent decrease in cell rolling-timesteps for all tested degradation rates (Fig. 8a). This is likely due to the dependence of EC E- and P-selectin expression on plasma cytokine levels. Forcing WSS to be uniform throughout the network and varying the magnitude showed an interesting pattern of total extravasation that could be explained by our rule set. The increased integrin affinity with increasing WSS explains the increase of extravasation at high WSS, while the increased EC expression of ICAM-1 and VCAM-1 at low shear levels explains the increase in extravasation at low WSS (Fig. 7b). Doubling or halving the control WSS showed expected results that could be explained by crossing of the maximum shear threshold for adhesion in the arterioles (Fig. 7b). Rolling also changed in an expected pattern, because of the increased likelihood of rolling at moderate shear values (Fig. 8). Finally, varying the rate of wall surveying by non-rolling monocytes showed significant differences in both rolling and extravasation between all groups (Figs. 7c and 8c). We performed trials with this surveying rate based on the ratio of segment flow velocity to rolling velocity and with a uniform surveying rate varied by two orders of magnitude. The model is extremely sensitive to changes in this parameter, and both this data and spatial extravasation patterns (not shown) suggest that the location and amount of monocyte rolling and extravasation is highly dependent on the rate and location of wall surveying.

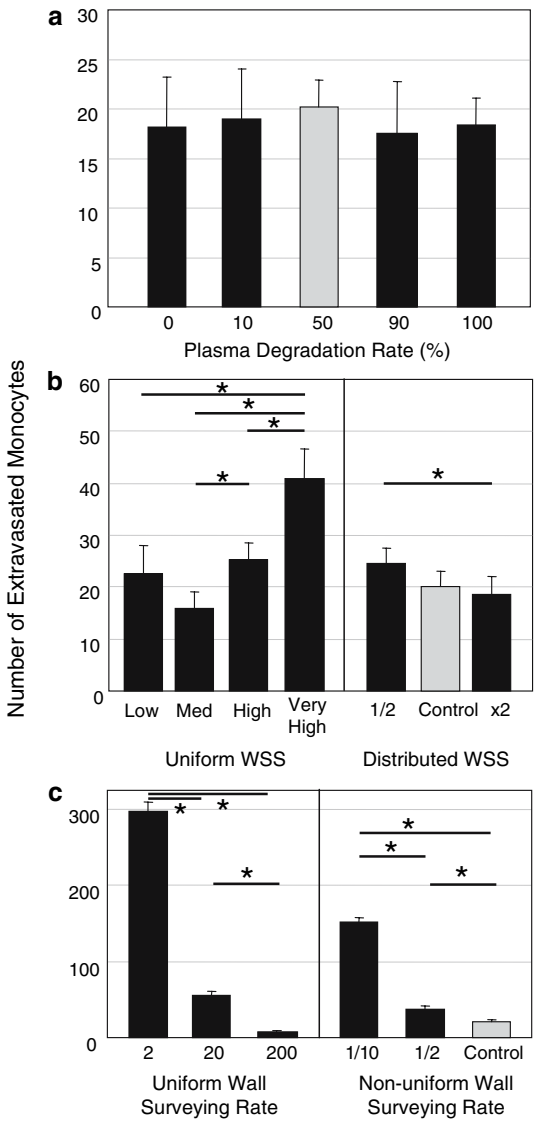

FIGURE 7. Analysis of the sensitivity of monocyte extravasation to plasma protein degradation rate, WSS, and wall surveying rate. (a) Variation of the plasma protein degradation rate from 0 to 100% per timestep showed no differences in extravasated monocytes. (b) Forcing WSS to be uniform throughout the network and modifying the distributed (non-uniform) control values showed significant ($p < 0.05$) dependence of extravasation on shear levels. (c) Variation of the wall surveying rate for non-rolling monocytes showed large significant differences in extravasation, underscoring the importance of this parameter (±SD; * = statistically significant relative to what the horizontal bars indicate with $p \leq 0.05$).

We also examined the sensitivity to knockout of the chemokine IL-8 and NO. As expected, IL-8 knockout produces a significant decrease ($p = 0.008$, data not

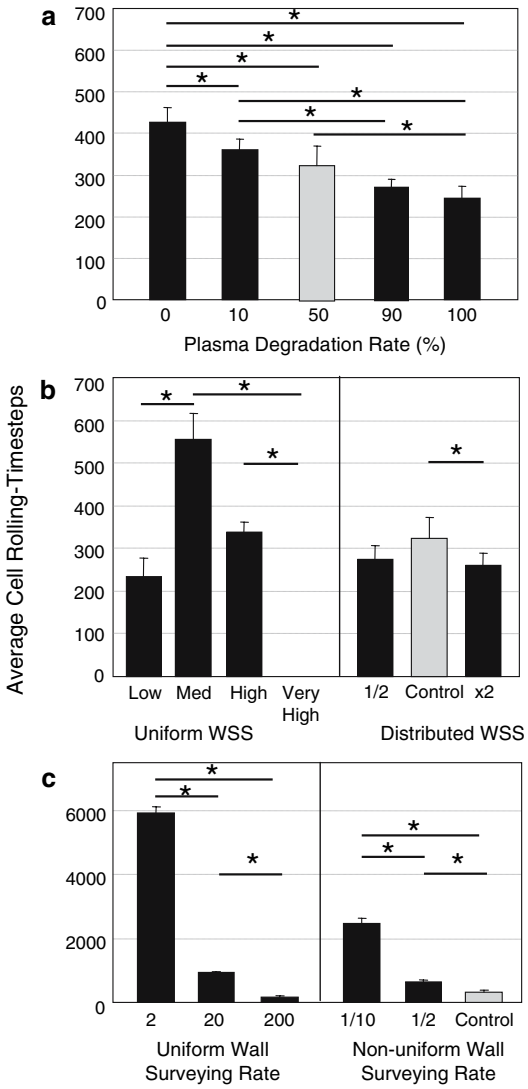

FIGURE 8. Analysis of the sensitivity of monocyte rolling (reported in Cell Rolling-Timesteps) to plasma protein degradation rate, WSS, and wall surveying rate. (a) Increasing the plasma protein degradation rate from 0 to 100% caused significant decreases in rolling. (b) Forcing WSS to be uniform throughout the network and modifying the distributed control values showed the expected dependence of cell rolling on WSS. (c) As the interval between wall surveys increased, the amount of monocyte rolling decreased significantly (±SD; * = statistically significant relative to what the horizontal bars indicate with $p \leq 0.05$).

shown) in the number of extravasated monocytes, while producing no change in the rolling behavior. At the current implementation state of NO, removal produces no significant change in either extravasation or rolling (data not shown).

DISCUSSION

We have developed an agent-based simulation of leukocyte trafficking through the microcirculation that spans multi-cell to tissue levels of biological scale in order to study the molecular mediators of the circulating cell adhesion cascade. Circulating monocytes and microvascular ECs are simulated on an individual-cell basis, and cells are programmed to respond to local mechanical and biochemical cues that drive monocyte rolling, adhesion, and transmigration into the tissue. The initial geometry and anatomy of the simulated microvascular network were obtained from a real microvascular network in a mouse spinotrapezius muscle. Individual cell behaviors are a dynamic response to a rule-set that was derived from independent literature, and the simulation output is the emergent accumulation of circulating monocyte-derived macrophages in the tissue. This process is relevant to many different disease states where inflammation is a key factor in the injury and recovery responses of the tissue.

The agent-based computational model is underpinned by a network flow analysis that calculates theoretical flow rates and pressures throughout the microvascular tree, while considering a variable blood viscosity. These predicted values, in turn, dictate how monocytes flow through the network and impact adhesion molecule expression and chemokine secretion. Our network blood flow model is based on Pries and Secomb's early work, although an important next step in the evolution of our computational framework is to incorporate aspects of an improved version of this model published in 2005.[90] Here, the authors modified their equations slightly to take into effect an endothelial cell surface layer (ESL) that served to reduce observed *in vivo* vessel diameters by a variable ESL thickness. Additionally, the incorporation of flow disturbances and capillary plugging caused by individual or small populations of leukocytes flowing through small vessels will likely be added to future models that consider ischemic interventions, mechanical wounding, and/or systemic or local inflammatory responses.

It should be re-emphasized here that SMCs are included for visual effect only, and have no behavioral rules. Because of this limitation, our implementation of the effects and production of NO is demonstrably incomplete. Incorporation of the behaviors of SMCs and additional sources and effects of NO are an important future target in our modeling process.

Another point that will be addressed as the model evolves is the assumption that cell surface expression of adhesion molecules is binary: either on or off. We acknowledge that this is not the case *in vivo*, and that varying levels of protein expression are important. However, it is technically challenging to accurately measure the levels of a receptor *in vivo*, and elucidating the response of a single cell to both varying levels of receptor expression and varying ligand concentrations

in vivo is currently impossible with the available assays. MacGabhann and Popel have pioneered a computational approach to this problem[70,71] which may be examined in future models. For the present work, considering cell surface protein expression as binary preserves the connections between molecules and provides high enough resolution to predict outcomes of selectin and integrin knockouts that are in agreement with the literature.

As a first step toward validating this integrated model, we performed a series of *in silico* knockout experiments, wherein individual and combinations of molecules were removed from the simulation by systematically altering the rule-set. The impacts these perturbations had on the number of extravasated macrophages in the tissue, the number of rolling cells, and the number of adherent cells were quantified. The data indicated a prominent role for ICAM-1 and VCAM-1 in monocyte rolling and adhesion, and a less important role for the selectins in these processes. These results are consistent with independent experimental studies performed in the corresponding set of knockout mice,[26,42] suggesting that our simulation is capable of independently predicting key events during monocyte trafficking.

A common pitfall in the design of ABMs is the fallacy of "programming the proof," or claiming that an outcome that was hardwired into the model from the start represents a validation of the model. In that case, the outcome is not a validation; the model simply outputs exactly what it was programmed to output. With this in mind, we developed a model of monocyte trafficking in skeletal muscle that preserves multiple levels of complexity with direct and indirect effects. For example, our rule-set states that E-selectin ligation has no direct effect on the activation of the $\beta 2$ integrins (MAC-1 and LFA-1). Simply put, there is no intracellular cross talk between the binding partner of E-selectin (PSGL-1) and the $\beta 2$ integrins that would lead to affinity changes. This does not exclude other indirect and potentially powerful effects of E-selectin on integrin activation through other pathways. Through studying the biology and the theoretical framework of our model, the existence of at least one alternate pathway is readily apparent: (1) selectin knockout leads to decreased rolling of monocytes along the endothelium; (2) a lack of cell rolling impacts velocity and leads to decreased wall surveying; (3) decreased wall surveying translates to fewer opportunities for integrin activation to occur (e.g., affinity changes induced by IL-8 exposure are less frequent); and (4) lower average integrin affinity decreases firm adhesion. Therefore, because of this and other pathways, the decreased dependence on selectins for monocyte capture, arrest, and extravasation is a non-intuitive result that was not programmed into the model, and a qualitative validation against *in vivo* data is possible.

Several other groups have modeled varying aspects of leukocyte–endothelium interactions, although none have integrated adhesion molecule expression with mechanical and biochemical signaling throughout the entire adhesion cascade. Krasik *et al.* elegantly integrated two types of modeling, mechanics-based and signaling-based, to elucidate and predict how integrin activating stimuli (e.g., E-selectin ligation) translated into neutrophil adhesion dynamics such as rolling time and distance traveled.[50] Other computational models have demonstrated that there are numerous determinants of cell rolling velocities, in addition to a receptor's affinity for its ligand.[49] Previous work has predicted the effects of leukocyte deformability on adhesion kinetics,[18,39] as well as the kinetics of integrin and L-selectin mediated neutrophil aggregation under flow.[107] All of these computational models are highly detailed and mechanistically informative, but they neglect the overall spatial and temporal dynamics within entire tissues. Thus, our model fills a critical gap and provides a tool to interrogate the individual and combined effects of molecules, cell behaviors, and mechanical forces. Useful extensions of this approach include combining it with intracellular signaling network models[82] such that each cell is underpinned by its own signaling network,[83] in order to expand the range of biological scales accounted for and to provide more fine-grained resolution of molecular signaling details within each cell. Furthermore, building onto the current framework through modular additions of other computational analysis techniques, including probabilistic models, neural networks, or more rigorous differential equations would allow for more powerful analysis.

Even though intracellular levels of detail are sacrificed in this first-attempt, we have shown that this computational approach can interrogate inflammatory cell trafficking mechanisms (and combinations of mechanisms) on a tissue-level scale. Although we only consider monocyte trafficking in a simulation that does not include an exhaustive list of adhesion molecules and chemokines/cytokines, the potential to expand the simulation is great. With this computational framework in place, the ability to extend the list of biochemical activators is immediately feasible, as new molecules and interactions are identified and new questions arise. Moreover, the ability to modify the simulation so as to incorporate additional cell types, including neutrophils, lymphocytes, and even circulating stem/progenitor cells, is promising. A new population of cells would likely respond to a similar set of rules, but differ in their population density, expression levels, and sensitivity to biochemical stimuli. With this

incorporation, it would be possible to compare the dependence of monocytes on the selectins to the dependence of neutrophils on the selectins.

By adding a simulated population of circulating stem/progenitor cells, either therapeutically delivered intravenously or mobilized from the bone marrow, it would be possible to test hypotheses regarding stem cell trafficking and incorporation into injured tissues. In this way, our simulation could be adapted to address a major question in regenerative medicine which centers on the role of circulating progenitor cells in angiogenesis: what signals and combinations thereof orchestrate their dynamic trafficking to injured tissues? By providing rules for EC proliferation (capillary sprouting) and by allowing intermittent hemodynamic flow/WSS updates from the network flow simulation during the execution of the agent-based simulation, an angiogenic microvascular network could be simulated. Then, the dynamic trafficking of circulating stem/progenitor cells during angiogenesis could be assessed and systematically manipulated within the setting of a simulated angiogenic microvascular network.

In summary, we have developed a computational model that captures the multi-cell tissue-level dynamics of monocyte trafficking within a microvascular network bed. Our model enables individual simulated cell tracking in space and time, which is currently not possible in experimental models. With the added ability to target specific molecules individually (e.g., by augmenting or decreasing their expression/functionality) we anticipate that this tool will serve as a platform not only for hypothesis testing, but also for hypothesis generation in a field that is of central importance to human disease and regenerative medicine.

ACKNOWLEDGMENTS

We are very grateful for the contributions of Kelly Benedict (University of Virginia, Department of Biomedical Engineering) for her help in the development of the network blood flow model. We are also grateful to Melissa Yingling for her contributions in the early developmental stages of this approach.

REFERENCES

[1]Abe, Y., C. M. Ballantyne, and C. W. Smith. Functions of domain 1 and 4 of vascular cell adhesion molecule-1 in alpha4 integrin-dependent adhesion under static and flow conditions are differentially regulated. *J. Immunol.* 157:5061–5069, 1996.

[2]Alon, R., S. Chen, R. Fuhlbrigge, K. D. Puri, and T. A. Springer. The kinetics and shear threshold of transient and rolling interactions of l-selectin with its ligand on leukocytes. *Proc. Natl. Acad. Sci. USA* 95:11631–11636, 1998.

[3]An, G. In silico experiments of existing and hypothetical cytokine-directed clinical trials using agent-based modeling. *Crit. Care. Med.* 32:2050–2060, 2004.

[4]Ando, J., H. Tsuboi, R. Korenaga, Y. Takada, N. Toyama-Sorimachi, M. Miyasaka, and A. Kamiya. Shear stress inhibits adhesion of cultured mouse endothelial cells to lymphocytes by downregulating vcam-1 expression. *Am. J. Physiol.* 267:C679–C687, 1994.

[5]Aziz, K. E., and D. Wakefield. Modulation of endothelial cell expression of icam-1, e-selectin, and vcam-1 by beta-estradiol, progesterone, and dexamethasone. *Cell Immunol.* 167:79–85, 1996.

[6]Ball, R. Y., E. C. Stowers, J. H. Burton, N. R. Cary, J. N. Skepper, and M. J. Mitchinson. Evidence that the death of macrophage foam cells contributes to the lipid core of atheroma. *Atherosclerosis* 114:45–54, 1995.

[7]de Boer, O. J., A. C. van der Wal, P. Teeling, and A. E. Becker. Leucocyte recruitment in rupture prone regions of lipid-rich plaques: a prominent role for neovascularization?. *Cardiovasc. Res.* 41:443–449, 1999.

[8]Capoccia, B.J., R.M. Shepherd, and D.C. Link. G-csf and amd3100 mobilize monocytes into the blood that stimulate angiogenesis *in vivo* through a paracrine mechanism. *Blood*, 2006.

[9]Chen, S., R. Alon, R. C. Fuhlbrigge, and T. A. Springer. Rolling and transient tethering of leukocytes on antibodies reveal specializations of selectins. *Proc. Natl. Acad. Sci. USA* 94:3172–3177, 1997.

[10]Chiu, J. J., P. L. Lee, C. N. Chen, C. I. Lee, S. F. Chang, L. J. Chen, S. C. Lien, Y. C. Ko, S. Usami, and S. Chien. Shear stress increases icam-1 and decreases vcam-1 and e-selectin expressions induced by tumor necrosis factor-[alpha] in endothelial cells. *Arterioscler. Thromb. Vasc. Biol.* 24:73–79, 2004.

[11]Chukwuemeka, A. O., K. A. Brown, G. E. Venn, and D. J. Chambers. Changes in p-selectin expression on cardiac microvessels in blood-perfused rat hearts subjected to ischemia-reperfusion. *Ann. Thorac. Surg.* 79:204–211, 2005.

[12]Coisne, C., C. Faveeuw, Y. Delplace, L. Dehouck, F. Miller, R. Cecchelli, and B. Dehouck. Differential expression of selectins by mouse brain capillary endothelial cells in vitro in response to distinct inflammatory stimuli. *Neurosci. Lett.* 392:216–220, 2006.

[13]Damiano, E. R., J. Westheider, A. Tozeren, and K. Ley. Variation in the velocity, deformation, and adhesion energy density of leukocytes rolling within venules. *Circ. Res.* 79:1122–1130, 1996.

[14]De Caterina, R., P. Libby, H. B. Peng, V. J. Thannickal, T. B. Rajavashisth, M. A. Gimbrone Jr, W. S. Shin, and J. K. Liao. Nitric oxide decreases cytokine-induced endothelial activation. Nitric oxide selectively reduces endothelial expression of adhesion molecules and proinflammatory cytokines. *J. Clin. Invest.* 96:60–68, 1995.

[15]Diamond, M. S., D. E. Staunton, S. D. Marlin, and T. A. Springer. Binding of the integrin mac-1 (cd11b/cd18) to the third immunoglobulin-like domain of icam-1 (cd54) and its regulation by glycosylation. *Cell* 65:961–971, 1991.

[16]Di Iorio, A., L. Ferrucci, E. Sparvieri, A. Cherubini, S. Volpato, A. Corsi, M. Bonafe, C. Franceschi, G. Abate, and R. Paganelli. Serum il-1beta levels in health and disease: a population-based study. 'the inchianti study'. *Cytokine* 22:198–205, 2003.

[17]DiVietro, J. A., M. J. Smith, B. R. Smith, L. Petruzzelli, R. S. Larson, and M. B. Lawrence. Immobilized il-8 triggers progressive activation of neutrophils rolling in vitro on p-selectin and intercellular adhesion molecule-1. *J. Immunol.* 167:4017–4025, 2001.

[18]Dong, C., J. Cao, E. J. Struble, and H. H. Lipowsky. Mechanics of leukocyte deformation and adhesion to endothelium in shear flow. *Ann. Biomed. Eng.* 27:298–312, 1999.

[19]Dunne, J. L., R. G. Collins, A. L. Beaudet, C. M. Ballantyne, and K. Ley. Mac-1, but not lfa-1, uses intercellular adhesion molecule-1 to mediate slow leukocyte rolling in tnf-alpha-induced inflammation. *J. Immunol.* 171:6105–6111, 2003.

[20]Dustin, M. L., R. Rothlein, A. K. Bhan, C. A. Dinarello, and T. A. Springer. Induction by il 1 and interferon-gamma: tissue distribution, biochemistry, and function of a natural adherence molecule (icam-1). *J. Immunol.* 137:245–254, 1986.

[21]Egami, K., T. Murohara, M. Aoki, and T. Matsuishi. Ischemia-induced angiogenesis: Role of inflammatory response mediated by p-selectin. *J. Leukoc. Biol.* 79:971–976, 2006.

[22]Elangbam, C. S., C. W. Qualls, and R. R. Dahlgren. Cell adhesion molecules-update. *Vet. Pathol.* 34:61–73, 1997.

[23]Elices, M. J., L. Osborn, Y. Takada, C. Crouse, S. Luhowskyj, M. E. Hemler, and R. R. Lobb. Vcam-1 on activated endothelium interacts with the leukocyte integrin vla-4 at a site distinct from the vla-4/fibronectin binding site. *Cell* 60:577–584, 1990.

[24]Finger, E. B., K. D. Puri, R. Alon, M. B. Lawrence, U. H. von Andrian, and T. A. Springer. Adhesion through l-selectin requires a threshold hydrodynamic shear. *Nature* 379:266–269, 1996.

[25]Frangogiannis, N. G. Targeting the inflammatory response in healing myocardial infarcts. *Curr. Med. Chem.* 13:1877–1893, 2006.

[26]Frenette, J., N. Chbinou, C. Godbout, D. Marsolais, and P. S. Frenette. Macrophages, not neutrophils, infiltrate skeletal muscle in mice deficient in p/e selectins after mechanical reloading. *Am. J. Physiol. Regul. Integr. Comp. Physiol.* 285:R727–732, 2003.

[27]van Furth, R., and Z. A. Cohn. The origin and kinetics of mononuclear phagocytes. *J. Exp. Med.* 128:415–435, 1968.

[28]Gonzales, R. S., and T. M. Wick. Hemodynamic modulation of monocytic cell adherence to vascular endothelium. *Ann. Biomed. Eng.* 24:382–393, 1996.

[29]Gopalan, P. K., C. W. Smith, H. Lu, E. L. Berg, L. V. McIntire, and S. I. Simon. Neutrophil cd18-dependent arrest on intercellular adhesion molecule 1 (icam-1) in shear flow can be activated through l-selectin. *J. Immunol.* 158:367–375, 1997.

[30]Hammer, D. A. Leukocyte adhesion: what's the catch?. *Curr. Biol.* 15:R96–R99, 2005.

[31]Haraldsen, G., D. Kvale, B. Lien, I. N. Farstad, and P. Brandtzaeg. Cytokine-regulated expression of e-selectin, intercellular adhesion molecule-1 (icam-1), and vascular cell adhesion molecule-1 (vcam-1) in human microvascular endothelial cells. *J. Immunol.* 156:2558–2565, 1996.

[32]Harris, A. G., and T. C. Skalak. Effects of leukocyte capillary plugging in skeletal muscle ischemia-reperfusion injury. *Am. J. Physiol.* 271:H2653–H2660, 1996.

[33]Hashimoto, K., N. Kataoka, E. Nakamura, H. Asahara, Y. Ogasawara, K. Tsujioka, and F. Kajiya. Direct observation and quantitative analysis of spatiotemporal dynamics of individual living monocytes during transendothelial migration. *Atherosclerosis* 177:19–27, 2004.

[34]Hemler, M. E., M. J. Elices, C. Parker, and Y. Takada. Structure of the integrin vla-4 and its cell-cell and cell-matrix adhesion functions. *Immunol. Rev.* 114:45–65, 1990.

[35]Hemler, M. E., C. Huang, Y. Takada, L. Schwarz, J. L. Strominger, and M. L. Clabby. Characterization of the cell surface heterodimer vla-4 and related peptides. *J. Biol. Chem.* 262:11478–11485, 1987.

[36]Hughes, J. M., A. Brink, A. N. Witmer, M. Hanraads-de Riemer, I. Klaassen, and R. O. Schlingemann. Vascular leucocyte adhesion molecules unaltered in the human retina in diabetes. *Br. J. Ophthalmol.* 88:566–572, 2004.

[37]Hwang, Y. S., M. Jeong, J. S. Park, M. H. Kim, D. B. Lee, B. A. Shin, N. Mukaida, L. M. Ellis, H. R. Kim, B. W. Ahn, and Y. D. Jung. Interleukin-1beta stimulates il-8 expression through map kinase and ros signaling in human gastric carcinoma cells. *Oncogene* 23:6603–6611, 2004.

[38]Jackson, L. A., D. A. Drevets, Z. M. Dong, R. A. Greenfield, and J. W. Murphy. Levels of l-selectin (cd62l) on human leukocytes in disseminated cryptococcosis with and without associated hiv-1 infection. *J. Infect. Dis.* 191:1361–1367, 2005.

[39]Jadhav, S., C. D. Eggleton, and K. Konstantopoulos. A 3-d computational model predicts that cell deformation affects selectin-mediated leukocyte rolling. *Biophys. J.* 88:96–104, 2005.

[40]Jiang, Z., S. A. Berceli, C. L. Pfahnl, L. Wu, D. Goldman, M. Tao, M. Kagayama, A. Matsukawa, and C. K. Ozaki. Wall shear modulation of cytokines in early vein grafts. *J. Vasc. Surg.* 40:345–350, 2004.

[41]Jung, U., D. C. Bullard, T. F. Tedder, and K. Ley. Velocity differences between l- and p-selectin-dependent neutrophil rolling in venules of mouse cremaster muscle in vivo. *Am. J. Physiol.* 271:H2740–H2747, 1996.

[42]Jung, U., and K. Ley. Mice lacking two or all three selectins demonstrate overlapping and distinct functions for each selectin. *J. Immunol.* 162:6755–6762, 1999.

[43]Kadambi, A., and T. C. Skalak. Role of leukocytes and tissue-derived oxidants in short-term skeletal muscle ischemia-reperfusion injury. *Am. J. Physiol. Heart. Circ. Physiol.* 278:H435–H443, 2000.

[44]Kern, S., S. A. Robertson, V. J. Mau, and S. Maddocks. Cytokine secretion by macrophages in the rat testis. *Biol. Reprod.* 53:1407–1416, 1995.

[45]Kim, M. B., and I. H. Sarelius. Role of shear forces and adhesion molecule distribution on p-selectin-mediated leukocyte rolling in postcapillary venules. *Am. J. Physiol. Heart. Circ. Physiol.* 287:H2705–H2711, 2004.

[46]Kloner, R. A., and R. B. Jennings. Consequences of brief ischemia: stunning, preconditioning, and their clinical implications: Part 2. *Circulation* 104:3158–3167, 2001.

[47]Kloner, R. A., and R. B. Jennings. Consequences of brief ischemia: stunning, preconditioning, and their clinical implications: Part 1. *Circulation* 104:2981–2989, 2001.

[48]Kofler, S., T. Nickel, and M. Weis. Role of cytokines in cardiovascular diseases: a focus on endothelial responses to inflammation. *Clin. Sci. (Lond.)* 108:205–213, 2005.

[49]Krasik, E. F., and D. A. Hammer. A semianalytic model of leukocyte rolling. *Biophys. J.* 87:2919–2930, 2004.
[50]Krasik, E. F., K. L. Yee, and D. A. Hammer. Adhesive dynamics simulation of neutrophil arrest with deterministic activation. *Biophys. J.* 91:1145–1155, 2006.
[51]Krishnaswamy, G., J. Kelley, L. Yerra, J. K. Smith, and D. S. Chi Human. Endothelium as a source of multifunctional cytokines: molecular regulation and possible role in human disease. *J. Interf. Cytok. Res.* 19:91–104, 1999.
[52]Krizanac-Bengez, L., M. Kapural, F. Parkinson, L. Cucullo, M. Hossain, M. R. Mayberg, and D. Janigro. Effects of transient loss of shear stress on blood-brain barrier endothelium: role of nitric oxide and il-6. *Brain Res.* 977:239–246, 2003.
[53]Lawrence, M. B., E. L. Berg, E. C. Butcher, and T. A. Springer. Rolling of lymphocytes and neutrophils on peripheral node addressin and subsequent arrest on icam-1 in shear flow. *Eur. J. Immunol.* 25:1025–1031, 1995.
[54]Lawrence, M. B., G. S. Kansas, E. J. Kunkel, and K. Ley. Threshold levels of fluid shear promote leukocyte adhesion through selectins (cd62l,p,e). *J. Cell. Biol.* 136:717–727, 1997.
[55]Lawrence, M. B., and T. A. Springer. Leukocytes roll on a selectin at physiologic flow rates: Distinction from and prerequisite for adhesion through integrins. *Cell* 65:859–873, 1991.
[56]Lawrence, M. B., and T. A. Springer. Neutrophils roll on e-selectin. *J. Immunol.* 151:6338–6346, 1993.
[57]Lee, Y. W., S. Y. Eum, K. C. Chen, B. Hennig, and M. Toborek. Gene expression profile in interleukin-4-stimulated human vascular endothelial cells. *Mol. Med.* 10:19–27, 2004.
[58]Leskinen, M. J., P. T. Kovanen, and K. A. Lindstedt. Regulation of smooth muscle cell growth, function and death in vitro by activated mast cells-a potential mechanism for the weakening and rupture of atherosclerotic plaques. *Biochem. Pharmacol.* 66:1493–1498, 2003.
[59]Ley, K. Molecular mechanisms of leukocyte recruitment in the inflammatory process. *Cardiovasc. Res.* 32:733–742, 1996.
[60]Ley, K. Integration of inflammatory signals by rolling neutrophils. *Immunol. Rev.* 186:8–18, 2002.
[61]Ley, K. Healing without inflammation?. *Am. J. Physiol. Regul. Integr. Comp. Physiol.* 285:R718–R719, 2003.
[62]Ley, K. The role of selectins in inflammation and disease. *Trend. Mol. Med.* 9:263–268, 2003.
[63]Ley, K., M. Allietta, D. C. Bullard, and S. Morgan. Importance of e-selectin for firm leukocyte adhesion in vivo. *Circ. Res.* 83:287–294, 1998.
[64]Li, S., B. Zhou, and Z. C. Han. Therapeutic neovascularization by transplantation of mobilized peripheral blood mononuclear cells for limb ischemia. A comparison between cd34+ and cd34− mononuclear cells. *Thromb. Haemost.* 95:301–311, 2006.
[65]Liang, F., N. Huang, B. Wang, H. Chen, and L. Wu. Shear stress induces interleukin-8 mrna expression and transcriptional activation in human vascular endothelial cells. *Chin. Med. J. (Engl.)* 115:1838–1842, 2002.
[66]Lobb, R. R., and M. E. Hemler. The pathophysiologic role of alpha 4 integrins in vivo. *J. Clin. Invest.* 94:1722–1728, 1994.
[67]Locksley, R. M., F. P. Heinzel, H. M. Shepard, J. Agosti, T. E. Eessalu, B. B. Aggarwal, and J. M. Harlan. Tumor necrosis factors alpha and beta differ in their capacities to generate interleukin 1 release from human endothelial cells. *J. Immunol.* 139:1891–1895, 1987.
[68]Longo, D., S. M. Peirce, T. C. Skalak, L. Davidson, M. Marsden, B. Dzamba, and D. W. DeSimone. Multicellular computer simulation of morphogenesis: blastocoel roof thinning and matrix assembly in xenopus laevis. *Dev. Biol.* 271:210–222, 2004.
[69]Lum, A. F., C. E. Green, G. R. Lee, D. E. Staunton, and S. I. Simon. Dynamic regulation of lfa-1 activation and neutrophil arrest on intercellular adhesion molecule 1 (icam-1) in shear flow. *J. Biol. Chem.* 277:20660–20670, 2002.
[70]Mac Gabhann, F., and A. S. Popel. Differential binding of vegf isoforms to vegf receptor 2 in the presence of neuropilin-1: a computational model. *Am. J. Physiol. Heart. Circ. Physiol.* 288:H2851–H2860, 2005.
[71]Mac Gabhann, F. and A. S. Popel. Interactions of vegf isoforms with vegfr1, vegfr2 and neuropilin in vivo: A computational model of human skeletal muscle. *Am. J. Physiol. Heart. Circ. Physiol.* 288:H2851–H2860, 2006.
[72]Marlin, S. D., and T. A. Springer. Purified intercellular adhesion molecule-1 (icam-1) is a ligand for lymphocyte function-associated antigen 1 (lfa-1). *Cell* 51:813–819, 1987.
[73]Masinovsky, B., D. Urdal, and W. M. Gallatin. Il-4 acts synergistically with il-1 beta to promote lymphocyte adhesion to microvascular endothelium by induction of vascular cell adhesion molecule-1. *J. Immunol.* 145:2886–2895, 1990.
[74]Moore, K. L., K. D. Patel, R. E. Bruehl, F. Li, D. A. Johnson, H. S. Lichenstein, R. D. Cummings, D. F. Bainton, and R. P. McEver. P-selectin glycoprotein ligand-1 mediates rolling of human neutrophils on p-selectin. *J. Cell. Biol.* 128:661–671, 1995.
[75]Morigi, M., C. Zoja, M. Figliuzzi, M. Foppolo, G. Micheletti, M. Bontempelli, M. Saronni, G. Remuzzi, and A. Remuzzi. Fluid shear stress modulates surface expression of adhesion molecules by endothelial cells. *Blood* 85:1696–1703, 1995.
[76]Muller, W. A., and G. J. Randolph. Migration of leukocytes across endothelium and beyond: Molecules involved in the transmigration and fate of monocytes. *J. Leukoc. Biol.* 66:698–704, 1999.
[77]Murfee, W. L., T. C. Skalak, and S. M. Peirce. Differential arterial/venous expression of ng2 proteoglycan in perivascular cells along microvessels: identifying a venule-specific phenotype. *Microcirculation* 12:151–160, 2005.
[78]Nagel, T., N. Resnick, W. J. Atkinson, C. F. Dewey Jr, and M. A. Gimbrone Jr. Shear stress selectively upregulates intercellular adhesion molecule-1 expression in cultured human vascular endothelial cells. *J. Clin. Invest.* 94:885–891, 1994.
[79]Neelamegham, S., A. D. Taylor, A. R. Burns, C. W. Smith, and S. I. Simon. Hydrodynamic shear shows distinct roles for lfa-1 and mac-1 in neutrophil adhesion to intercellular adhesion molecule-1. *Blood* 92:1626–1638, 1998.
[80]Nerem, R. M., R. W. Alexander, D. C. Chappell, R. M. Medford, S. E. Varner, and W. R. Taylor. The study of the influence of flow on vascular endothelial biology. *Am. J. Med. Sci.* 316:169–175, 1998.
[81]O'Neill IV, T. J. T., Wamhoff B. R., Owens G. K., Skalak T. C. 2005 Mobilization of bone marrow-derived cells enhances the angiogenic response to hypoxia without

transdifferentiation into endothelial cells. Circ. Res. 97:1027–1035.
[82]Papin, J. A., T. Hunter, B. O. Palsson, and S. Subramaniam. Reconstruction of cellular signalling networks and analysis of their properties. *Nat. Rev. Mol. Cell. Biol.* 6:99–111, 2005.
[83]Peirce, S. M., T. C. Skalak, and J. A. Papin. Coupling intracellular networks with tissue-level physiology. *IBM J. Res.* 50:1–55, 2006.
[84]Peirce, S. M., E. J. Van Gieson, and T. C. Skalak. Multicellular simulation predicts microvascular patterning and in silico tissue assembly. *Faseb. J.* 18:731–733, 2004.
[85]Pigott, R. and C. Power. The Adhesion Molecule Facts Book. Factsbook series. New York: Harcourt Brace & Company, Publishers, 190, 1993.
[86]Polley, M. J., M. L. Phillips, E. Wayner, E. Nudelman, A. K. Singhal, S. Hakomori, and J. C. Paulson. Cd62 and endothelial cell-leukocyte adhesion molecule 1 (elam-1) recognize the same carbohydrate ligand, sialyl-lewis x. *Proc. Natl. Acad. Sci. USA* 88:6224–6228, 1991.
[87]Porsch-Oezcueruemez, M., D. Kunz, H. U. Kloer, and C. Luley. Evaluation of serum levels of solubilized adhesion molecules and cytokine receptors in coronary heart disease. *J. Am. Coll. Cardiol.* 34:1995–2001, 1999.
[88]Prabhakarpandian, B., D. J. Goetz, R. A. Swerlick, X. Chen, and M. F. Kiani. Expression and functional significance of adhesion molecules on cultured endothelial cells in response to ionizing radiation. *Microcirculation* 8:355–364, 2001.
[89]Price, R. J., and T. C. Skalak. A circumferential stress-growth rule predicts arcade arteriole formation in a network model. *Microcirculation* 2:41–51, 1995.
[90]Pries, A. R., and T. W. Secomb. Microvascular blood viscosity in vivo and the endothelial surface layer. *Am. J. Physiol. Heart. Circ. Physiol.* 289:H2657–H2664, 2005.
[91]Pries, A. R., T. W. Secomb, P. Gaehtgens, and J. F. Gross. Blood flow in microvascular networks. Experiments and simulation. *Circ. Res.* 67:826–834, 1990.
[92]Pries, A. R., T. W. Secomb, T. Gessner, M. B. Sperandio, J. F. Gross, and P. Gaehtgens. Resistance to blood flow in microvessels in vivo. *Circ. Res.* 75:904–915, 1994.
[93]Ramos, C. L., Y. Huo, U. Jung, S. Ghosh, D. R. Manka, I. J. Sarembock, and K. Ley. Direct demonstration of p-selectin- and vcam-1-dependent mononuclear cell rolling in early atherosclerotic lesions of apolipoprotein e-deficient mice. *Circ. Res.* 84:1237–1244, 1999.
[94]Rose, D. M., J. Han, and M. H. Ginsberg. Alpha4 integrins and the immune response. *Immunol. Rev.* 186:118–124, 2002.
[95]Rothlein, R., M. L. Dustin, S. D. Marlin, and T. A. Springer. A human intercellular adhesion molecule (icam-1) distinct from lfa-1. *J. Immunol.* 137:1270–1274, 1986.
[96]Sabry, A., H. Sheashaa, A. El-Husseini, K. Mahmoud, K. F. Eldahshan, S. K. George, E. Abdel-Khalek, E. M. El-Shafey, and H. Abo-Zenah. Proinflammatory cytokines (tnf-alpha and il-6) in egyptian patients with sle: its correlation with disease activity. *Cytokine* 35:148–153, 2006.
[97]Sako, D., X. J. Chang, K. M. Barone, G. Vachino, H. M. White, G. Shaw, G. M. Veldman, K. M. Bean, T. J. Ahern, and B. Furie. Expression cloning of a functional glycoprotein ligand for p-selectin. *Cell* 75:1179–1186, 1993.
[98]Sarangapani, K. K., T. Yago, A. G. Klopocki, M. B. Lawrence, C. B. Fieger, S. D. Rosen, R. P. McEver, and C. Zhu. Low force decelerates l-selectin dissociation from p-selectin glycoprotein ligand-1 and endoglycan. *J. Biol. Chem.* 279:2291–2298, 2004.
[99]Seal, J. B., and B. L. Gewertz. Vascular dysfunction in ischemia-reperfusion injury. *Ann. Vasc. Surg.* 19:572–584, 2005.
[100]Setiadi, H., and R. P. McEver. Signal-dependent distribution of cell surface p-selectin in clathrin-coated pits affects leukocyte rolling under flow. *J. Cell. Biol.* 163:1385–1395, 2003.
[101]Shimada, Y., M. Hasegawa, K. Takehara, and S. Sato. Elevated serum l-selectin levels and decreased l-selectin expression on cd8(+) lymphocytes in systemic sclerosis. *Clin. Exp. Immunol.* 124:474–479, 2001.
[102]Simon, S. I., A. R. Burns, A. D. Taylor, P. K. Gopalan, E. B. Lynam, L. A. Sklar, and C. W. Smith. L-selectin (cd62l) cross-linking signals neutrophil adhesive functions via the mac-1 (cd11b/cd18) beta 2-integrin. *J. Immunol.* 155:1502–1514, 1995.
[103]Simon, S. I., and H. L. Goldsmith. Leukocyte adhesion dynamics in shear flow. *Ann. Biomed. Eng.* 30:315–332, 2002.
[104]Sperandio, M., M. L. Smith, S. B. Forlow, T. S. Olson, L. Xia, R. P. McEver, and K. Ley. P-selectin glycoprotein ligand-1 mediates l-selectin-dependent leukocyte rolling in venules. *J. Exp. Med.* 197:1355–1363, 2003.
[105]Springer, T. A. Traffic signals for lymphocyte recirculation and leukocyte emigration: the multistep paradigm. *Cell* 76:301–314, 1994.
[106]Swerlick, R. A., K. H. Lee, L. J. Li, N. T. Sepp, S. W. Caughman, and T. J. Lawley. Regulation of vascular cell adhesion molecule 1 on human dermal microvascular endothelial cells. *J. Immunol.* 149:698–705, 1992.
[107]Tandon, P., and S. L. Diamond. Kinetics of beta2-integrin and l-selectin bonding during neutrophil aggregation in shear flow. *Biophys. J.* 75:3163–3178, 1998.
[108]Van Gieson, E. J., W. L. Murfee, T. C. Skalak, and R. J. Price. Enhanced smooth muscle cell coverage of microvessels exposed to increased hemodynamic stresses in vivo. *Circ. Res.* 92:929–936, 2003.
[109]Wieczorowska-Tobis, K., Z. I. Niemir, R. Podkowka, K. Korybalska, M. Mossakowska, and A. Breborowicz. Can an increased level of circulating il-8 be a predictor of human longevity?. *Med. Sci. Monit.* 12:CR118–CR121, 2006.
[110]Wilensky, U. In: Netlogo, edited by N. University. Center for Connected Learning and Computer-based Modeling: Evanston, IL, 1999.
[111]Wilhelmi, M. H., R. G. Leyh, M. Wilhelmi, and A. Haverich. Upregulation of endothelial adhesion molecules in hearts with congestive and ischemic cardiomyopathy: immunohistochemical evaluation of inflammatory endothelial cell activation. *Eur. J. Cardiothorac. Surg.* 27:122–127, 2005.
[112]Wojciechowski, J. C., and I. H. Sarelius. Preferential binding of leukocytes to the endothelial junction region in venules in situ. *Microcirculation* 12:349–359, 2005.
[113]Xingyuan, M., Z. Wenyun, and W. Tianwen. Leukocyte function-associated antigen-1: structure, function and application prospects. *Protein Pept. Lett.* 13:397–400, 2006.
[114]Yago, T., J. Wu, C. D. Wey, A. G. Klopocki, C. Zhu, and R. P. McEver. Catch bonds govern adhesion through l-selectin at threshold shear. *J. Cell. Biol.* 166:913–923, 2004.
[115]Yoshida, A., H. K. Takahashi, M. Nishibori, H. Iwagaki, T. Yoshino, T. Morichika, M. Yokoyama, E. Kondo, T.

Akagi, and N. Tanaka. Il-18-induced expression of intercellular adhesion molecule-1 in human monocytes: involvement in il-12 and ifn-gamma production in pbmc. *Cell Immunol*. 210:106–115, 2001.

[116]Zwartz, G. J., A. Chigaev, D. C. Dwyer, T. D. Foutz, B. S. Edwards, and L. A. Sklar. Real-time analysis of very late antigen-4 affinity modulation by shear. *J. Biol. Chem*. 279:38277–38286, 2004.